Materials Research Proceedings 28 (2023) 855-865 https://doi.org/10.21741/9781644902479-94

Determination of the forming limit curve of locally annealed aluminum blanks

PICCININNI Antonio[1,a *], LATTANZI Attilio[2,b], ROSSI Marco[2,c] and PALUMBO Gianfranco[1,d]

[1]Department of Mechanical Engineering, Mathematics & Management Engineering, Division of Production Technologies, Polytecnic University of Bari, via Orabona 4, 70125 Bari, Italy

[2]Department of Industrial Engineering and Mathematical Sciences, Università Politecnica delle Marche, via Brecce Bianche 12, 60131 Ancona, Italy

[a]antonio.piccininni@poliba.it, [b] a.lattanzi@staff.univpm.it, [c]m.rossi@staff.univpm.it, [d]gianfranco.palumbo@poliba.it

Keywords: Laser Heat Treatment, Aluminum Alloy, FEM, FLC, Bulge Test

Abstract. The research of innovative manufacturing routes to improve the complexity of structural Aluminum (Al) components and reduce the vehicles' weight remains an open question. The adoption of short-term heat treatments to obtain an optimized distribution of properties has shown great potential in enhancing the formability of Al alloys at room temperature. Such a complex approach needs the implementation of methodologies based on numerical simulations able to correctly simulate the forming process. Accordingly, the definition of a proper identification procedure to provide reliable constitutive parameters, possibly employing a limited number of tests, becomes crucial. In this work, we introduce a novel methodology for the evaluation of the Forming Limit Curve (FLC) of laser annealed AA5752-H32 sheet based on the material information from different heterogeneous tests carried out in specific tribological condition, i.e. in absence of friction. Therefore, we investigate an experimental procedure to simultaneously generate an equi-biaxial mechanical state over a wide range of annealing conditions by means of hydraulic bulge test. The results are integrated with full-field data from uniaxial tensile and plane strain tests to provide a testing protocol for the characterization of the failure behavior accounting for the different temperature/time conditions of the sheet metal.

Introduction

The continuous demand for greener and lighter transportations is moving the attention to the improvement of the design criteria, among which the choice of the material for the structural components plays a key role. At the same time, it is widely recognized that Aluminum (Al) alloys are ranked as an ideal candidate to match those requirements [1]. Nevertheless, excellent fire resistance (especially when dealing with the subway applications [2]) combined with high strength-to-weight ratio are partially counterbalanced by the poor formability at room temperature [3]. Several solutions have been investigated over the last decades to overcome such a limitation: the increase of the working temperature – i.e. the theoretical base of the forming operations in warm conditions – has shown great potentialities over a large variety of components [4,5]. A promising and innovative alternative to the warm forming principle is based on splitting the manufacturing process into two separate steps: during the first phase, the material properties are locally modified by means of a short-term heat treatment (for example, by means of a laser heating) so that the blank, once cooled down, can be stamped at room temperature. It has been demonstrated that the optimization of the distribution of the material properties is able to enhance the formability at room temperature [6,7].

Splitting the process into two separate sub-steps automatically implies the need of a robust and systematic approach to design both the steps, especially due to the large number of parameters

involved in. Moreover, if the numerical approach is indicated as the most reliable methodology to design such a complex process, the proper characterization of the material behavior is a key aspect to be addressed to study in detail the mechanical response in the following forming operation.

While the effect of annealing on the constitutive behavior of the alloy can be investigated by considering, separately, samples of the same material treated at different grades, recently, the application of full-field measurements as the Digital Image Correlation (DIC) has allowed to disentangle the heterogeneous distribution of mechanical properties due to the local annealing [8, 18-20]. In this framework, dealing with heterogenous information makes possible to involve advanced calibration methods based on inverse problems. Generally, they are distinguished in numerical simulation-based methods, such as the Finite Element Model Updating (FEMU), and energy balance-based methods, namely the Virtual Fields Method (VFM) or the Equilibrium Gap Method (EGM) [11]. In the field of metal plasticity, inverse identification methods offer different strategies to produce an enriched calibrations even in the case of complex material models [23]: for instance, for the identification of the hardening behavior including post-necking data [13,14], or to characterize the anisotropic plasticity models [12,15,16] or the thermomechanical behavior of metals [17].

The present work investigates the stretching behavior of a locally laser-annealed AA5752-H32 sheet in a hydraulic bulge test. The aim is to provide heterogenous material data in the biaxial and equi-biaxial stretch conditions spanning over the whole annealing range, that can be coupled with an inverse approach as in [24], or to build a more comprehensive Forming Limit Curve. Different heating strategies have been preliminarily simulated by solving the thermal transient problem and the modification of the material properties have also been numerically predicted. The nodal peak temperatures, being strictly connected to the final level of annealing, were then transferred on the structural model, where the material behavior was modelled according to the hardening law that has been previously calibrated by the same authors [18]. The results, integrated with those coming from the plane strain [19] and from the drawing side, allow to provide a testing methodology to characterize the necking behavior at different material conditions using a limited number of tests.

Material and Methodology

Material.

Bulge tests were simulated considering locally modified AA5754 Al blanks, initially purchased in the H32 state, whose composition is reported in Table 1.

Table 1. Chemical composition of the investigated alloy.

	Al [%]	Cr [%]	Cu [%]	Fe [%]	Mg [%]	Mn [%]	Si [%]	Ti [%]	Zn [%]
AA5754-H32	Bal.	0.024	0.057	0.377	3.057	0.187	0.259	0.017	0.025

Annealing investigation.

The prediction of the material properties at the end of the local heating started from a preliminary characterization step based on the physical simulation of several annealing treatments exploiting the potentialities of the Gleeble system (model 3180). Dog-bone specimens (AA5754-H32) were subjected to a heat treatment composed of a preliminary heating step (rate around 900°C/s), holding at the test temperature and rapid cooling down to room temperature. Being the ends of the specimen clamped by cooled jaws, a parabolic distribution of temperatures occurs during the whole test (equivalent to simultaneously subjecting the same specimen to several heat treatments at the temperatures belonging to the parabolic distribution): hardness tests, carried out once the specimen cools down to room temperature, allowed to easily associate the modification of the material property to the temperature-time history. Hardness measurements were arranged in terms of the Ann variable variable according to Eq. 1: HV_{H32}, HV_{meas} and HV_{H111} refer to the

Materials Research Proceedings 28 (2023) 855-865 https://doi.org/10.21741/9781644902479-94

hardness of the material in the as-received conditions (H32), measured one and in the annealed state (H111), respectively.

$$Ann = \frac{HV_{H32} - HV_{meas}}{HV_{H32} - HV_{H111}} \tag{1}$$

The distribution of the defined variable, as well as its dependency with the peak temperature (T_{peak}), fitted by the sigmoid function, widely used in several applications [14], expressed in Eq. 2, where $\boldsymbol{T}^*$ and λ represents the curve's midpoint and growth rate (or steepness), respectively.

$$Ann = \frac{1}{1 + \exp\left[-\lambda \cdot \left(T^* - T_{peak}\right)\right]} \tag{2}$$

Although Eq. 2 offers a direct analytical description of the percentage of annealing due to the temperature distribution, it does not provide direct information about the different mechanical properties and, therefore, cannot be straightforwardly adopted in structural problems. In this sense, the authors proposed a constitutive model to predict the hardening behavior as function of the T_{peak}. By expressing the annealing level through the general variable T_{peak}, the corresponding flow curve can be predicted using the following logistic expression:

$$\sigma\left(\varepsilon_p, T_{peak}\right) = \sigma_{H111}\left(\varepsilon_p\right) + \frac{\sigma_{H32}\left(\varepsilon_p\right) - \sigma_{H111}\left(\varepsilon_p\right)}{1 + \exp\left\{-\left[\beta \tanh\left(\frac{\varepsilon_p}{\varepsilon_0}\right) + c_\beta\right]\left(T^* - T_{peak}\right)\right\}} \tag{3}$$

where ε_p is the accumulated plastic strain, the $\sigma_{H32}\left(\varepsilon_p\right)$ and $\sigma_{H111}\left(\varepsilon_p\right)$ indicates the flow curves of the material at H32 and fully-annealed (H111) conditions, respectively; β, ε_0, T^* and c_β are the material coefficients regulating the logistic expression. All the coefficients can be inversely calibrated by considering the flow stress curves at different annealing grades. Details about the calibration of the hardening model in Eq. 3 by using a hybrid numerical-experimental procedure on uniaxial tensile data can be found in [18].

Two-steps FE analysis of the heat-treatment and mechanical test.

The adopted approach started from the simulation of the laser heating by solving the thermal transient problem. The investigated heating strategies were based on: (i) a circular track described by the center of the laser spot (indicated by the red square in Fig. 1a) with a radius equal to 30 mm (labelled as AH, standing for *Annular Heating*) and (ii) a linear track, 40 mm long, at two different distances from the center of the blank (20 mm and 30 mm, respectively labelled as LT20 and LT30, where LT stands for *Linear Track*). The simulated strategies were designed to investigate the equi-biaxial stress state over different material conditions (the gradient of properties came from the local laser heating) within the same bulge test.

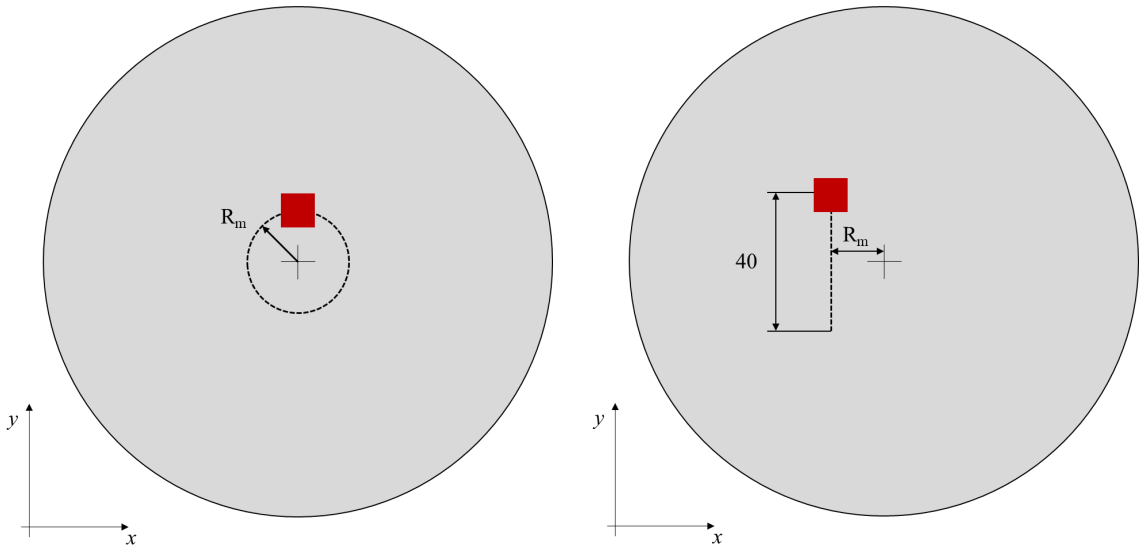

a) b)

Fig. 1. The investigated heating strategies: a) AH, b) LT. The diameter of the blank is 300 mm, while the gauge area has a diameter of 200 mm (corresponding to the die opening).

Laser heating strategies were simulated implementing a temperature feedback loop (DFLUX user subroutine), setting the heating temperature at 550°C and the feed rate at 5 mm/s. Results from the thermal simulations were processed by means of a Python script to numerically predict the final distribution of the variable *Ann* according to Eq. 2.

In this study, we consider the peak temperature T_{peak} as the common empirical variable to connect the predicted level of annealing with the hardening behavior. Thus, the computed T_{peak} from the transient-thermal analysis is used as input of the structural analysis through the constitutive model in Eq. 3. The forming bulge is replicated numerically by modelling the die as rigid body and the aluminum blank as continuum shell under the hypothesis of plane stress condition due to the small thickness of the sheet metal. Note that the constitutive equations were implemented in Abaqus/Standard® by means of a user material subroutine, employing the well-known Euler Backward integration algorithm for the reconstruction of stress from strain data. Other implicit or semi-implicit algorithms can be also used for the stress update as, for example, the one introduced in [22] for anisotropic plasticity problems.

In this work, we also assumed an isotropic plasticity behavior, while the hardening behavior of the AA5754 was described by using a modified version of the Voce's law, according to the previous experimental investigation reported in [18]:

$$\sigma(\varepsilon_p) = Y(1 + \varepsilon_p) - R\exp(-b\varepsilon_p). \quad (4)$$

All the material coefficients used in this numerical study, including the ones characterizing the logistic formulation in Eq. 3, are listed in Table 2.

Table 2. Material coefficient of the constitutive equation.

Modified Swift hardening law			
Material state	Y	R	b
As received (H32)	232.74	98.32	20.08
Fully annealed	213.36	148.53	26.99
Logistic hardening model			
β	c_β	T^*	ε_0
0.01095	0.01423	301.35	0.005

Results

Treatment strategies for the heterogeneous bulge test.

Results from the thermal simulations were initially analyzed in terms of maximum temperature distribution: Fig. 2 confirms that the heating temperature close to 550°C was reached and kept along the whole heat treatment in each of the investigated strategies.

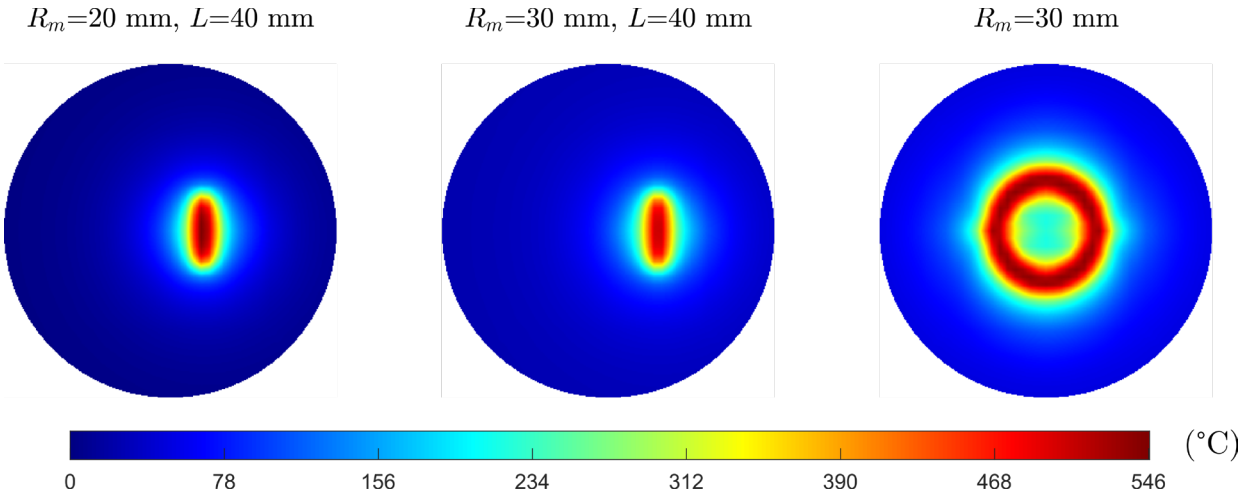

Fig. 2. Results from the transient-thermal analysis: distribution of the peak temperature T_{peak} for the three heat-treatment strategies.

The final distribution of properties, express in terms of the variable *Ann*, was compared among the three strategies along a radial path as shown in Fig. 3 (the *0* radial position corresponds to the center of the circular blank).

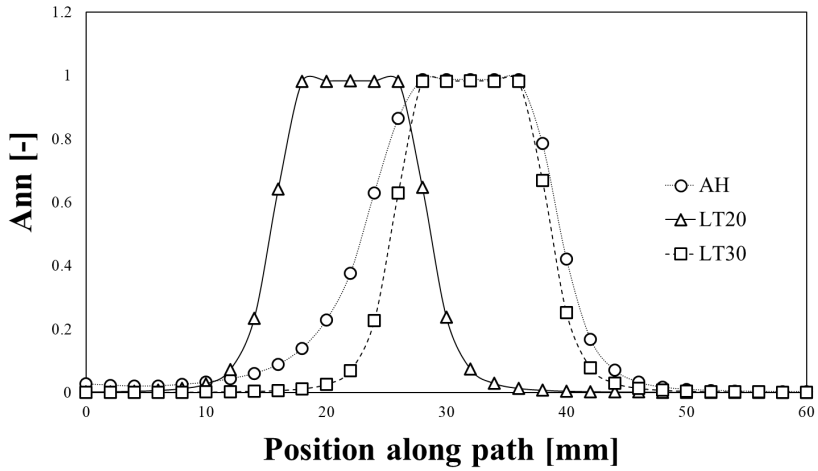

Fig. 3. Predicted distribution of the Ann variable along the radial

It can be observed that all the geometries show an almost complete annealing (*Ann* close to 1) in the region irradiated by the laser spot (around 10 mm wide in the radial direction). It can also be seen that the annular tracking (AH) modifies a slightly larger portion of the blank close to its center (the transition region is less steep if compared with the *Ann* distribution resulting from the LT30 strategy).

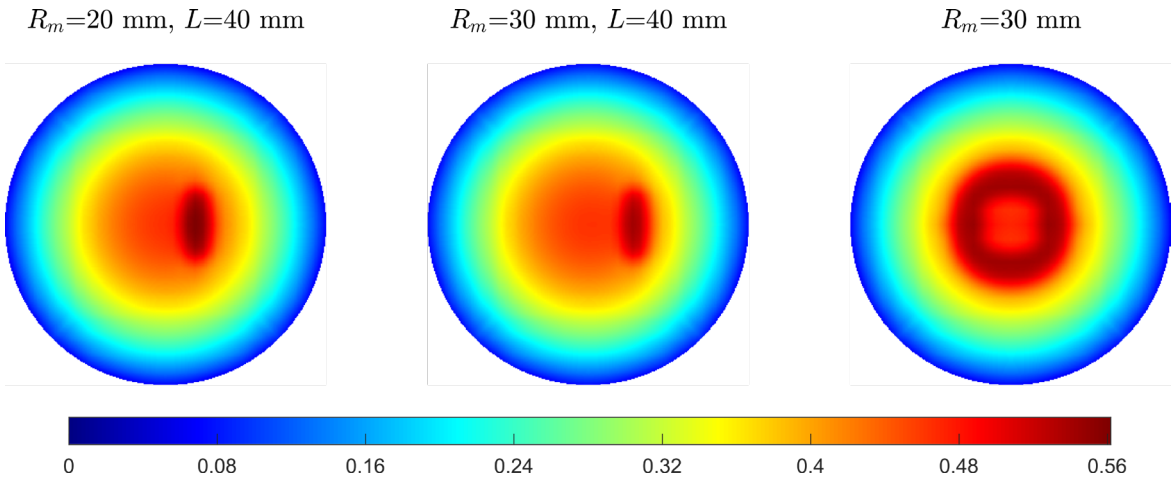

Fig. 4. Maps of accumulated equivalent plastic strain over the bulge test gauge area for the three heat-treatment strategies.

The design of a heterogenous test requires a quantitative method to classify the strain and stress distribution, that, for this study, must consider the annealing temperature and the amount of plastic deformation accumulated during the loading phase. Fig. 4 depicts the maximum plastic strain achieved in our simulated experiments. Note that we impose the same maximum forming pressure for each case study (4.4 MPa) to obtain comparable values of equivalent plastic strain $\bar{\varepsilon}_p$. In all the cases, the maximum $\bar{\varepsilon}_p$ obtained is around 0.56 and is located over the material points identified by the fully annealed condition, although they are quite far from the dome apex. It is worth noticing that, although we imposed the same target forming pressure to all the tests, obtaining similar values of maximum equivalent plastic strain, the macroscopic effect of the annealing treatment on the specimen can be observed on the maximum dome height, which is 60 mm for the LT strategy and 62 mm for the AH one.

To be consistent with previous studies aimed to quantify the heterogeneity of the mechanical states produced by unconventional mechanical test [19,25], the classification and comparison of the three strategies is carried out following two main visualization methods:

- The diagram of major and minor principal strains, also used to infer the FLC;
- The diagram of normalized stress (widely used in the case of anisotropic plasticity), where the stress state for each material point is reported on the yield surface.

It is worth noting that the following diagrams includes only datapoints where the $\bar{\varepsilon}_p > 2\%$: this because low values of plastic deformation – corresponding to low values of dome height – are strongly affected by uncertainties when measured with optical techniques as DIC.

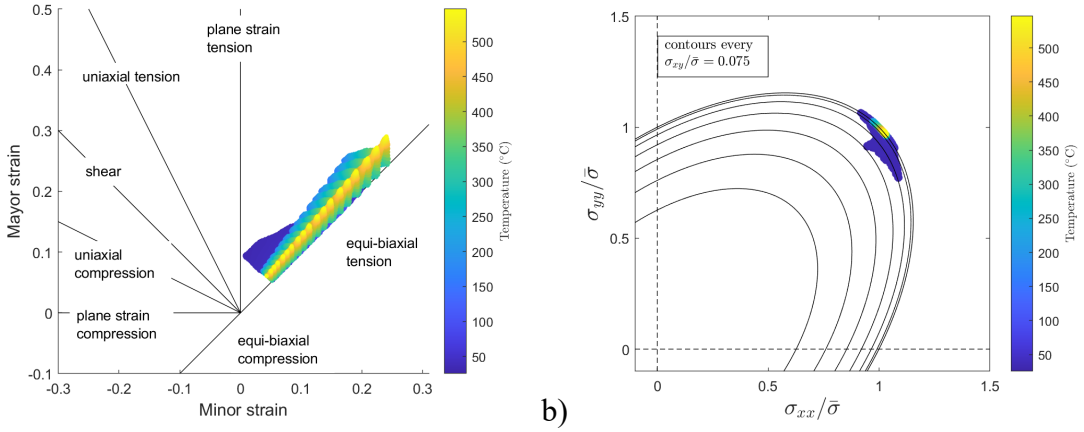

Fig. 5. Distribution of major and minor strains (a) and stress states on the normalized stress plane (b) produced by the bulge test on the specimen exposed to the linear treatment with R_m=20 mm and L=40 mm.

When looking at the results from the LT20, the forming limit diagram shown in Fig. 5a suggests that all the points close to the fully annealed state (yellow point) are characterized by a slope of the strain path slightly higher than that of the equi-biaxial state. On the other hand, material points characterized by lower level of annealing (peak temperature around 400°C) are closer to the bisector of the first quadrant. When moving far from the locally annealed zone, the strain path diverges from the equi-biaxial state more evidently.
The distance between the linear track and the center of the circular blank seems not to have an appreciable effect: in fact, when increasing the distance up to 30 mm, the evolution of the strain paths (Fig. 6a) resembles the distribution shown in Fig. 5a.

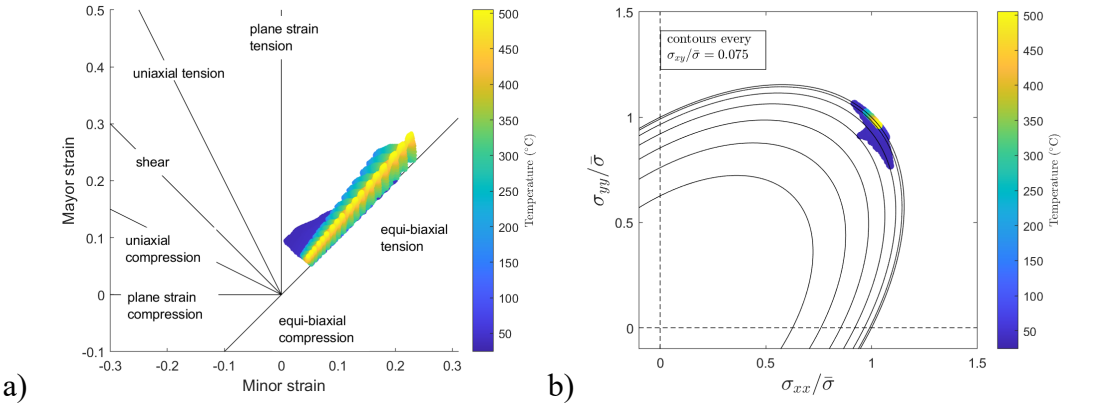

Fig. 6. Distribution of major and minor strains (a) and stress states on the normalized stress plane (b) produced by the bulge test on the specimen exposed to the linear treatment with R_m=30 mm and L=40 mm.

The evolution of the strain paths slightly changes when focusing the attention on the AH strategy. The scatter of the slope in the strain paths from the material point at the higher level of annealing is larger and a wider span of intermediate annealing conditions reaches the almost equi-biaxial state during the forming (Fig. 7, a and b).

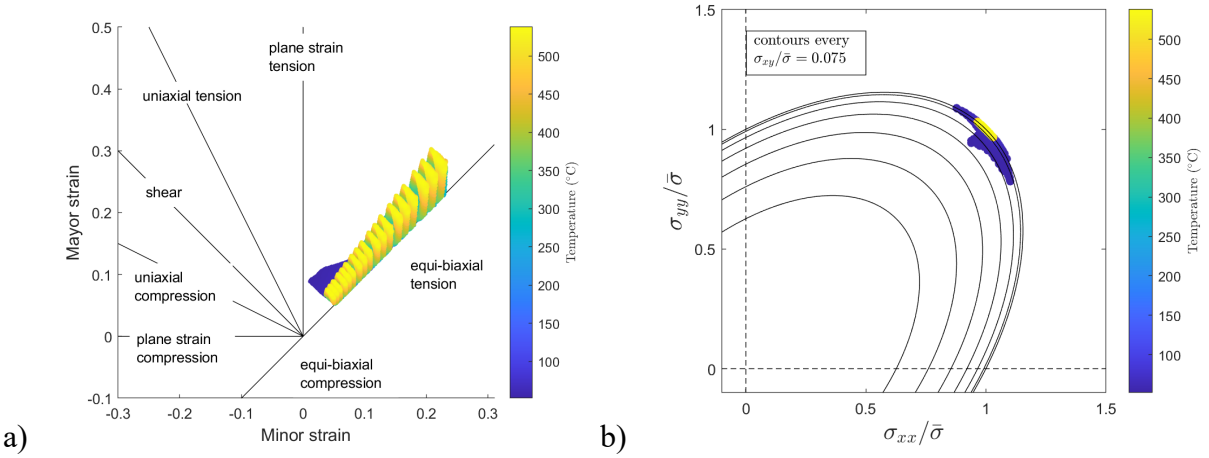

Fig. 7. Distribution of major and minor strains (a) and stress states on the normalized stress plane (b) produced by the bulge test on the specimen exposed to the circular treatment with R_m=30 mm.

The difference between the three investigated geometries are confirmed when looking at the strain paths from a radial path of nodes: for both the LT strategies, the points characterized by the fully annealed conditions, despite slightly diverging from the equi-biaxial state, reached a final strain condition higher than the other points characterized by intermediate levels of annealing (Fig. 8a and Fig. 8b).

On the other hand, when the AH strategy is taken into account, the final strain components (major and minor) are quite close regardless of the reached level of annealing.

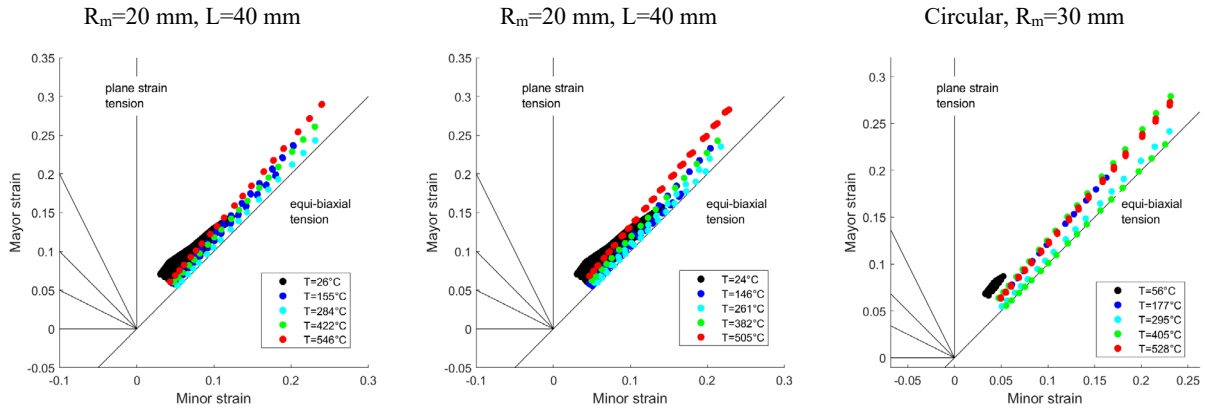

Fig. 8. Distribution of major and minor strains obtained by sampling measurement points along a horizontal path in the case of five annealing temperatures, for all the heat-treatment configurations.

FLC curve reconstruction from different heterogenous tests.

The strain path distributions from the locally annealed bulge tests, combined with the strain evolutions from the other two types of tests (tensile test and plane strain tests) allow to cover a wide portion of the forming limit diagrams. The onset of necking, particularly difficult to infer from the numerical simulation of the characterization tests (plane strain and bulge test) can be qualitatively drawn, embracing the limit conditions not only belonging to the material points in the fully annealed conditions but also some characterized by an intermediate level of annealing.

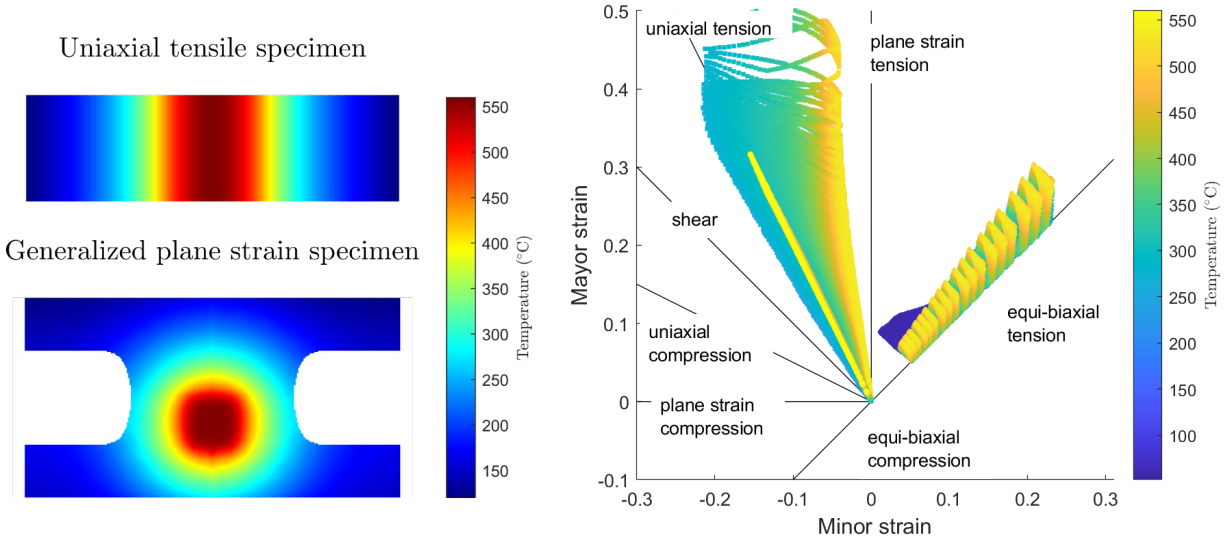

a) b)

Fig. 9. Integration of different heterogeneous tests with the bulge specimen exposed to circular heat-treatment: a) distribution of the peak temperature for the uniaxial and generalized plane strain specimens, b) combined FLC diagram including all full-field data.

Summary

The present work focuses the attention on the third characterization tests when considering a gradient of properties in a AA5754-H32 blank that has been locally annealed by means of laser heating. The simulation of the bulge test, in combination with the tensile and the plane strain tests, complete the set of characterization methodology to assess the strain behavior of a locally-modified blank. The three investigated laser heating, different in terms of extent of the annealed region (a single linear track against a circular path) seemed not to have a significant influence on the evolution of the slope of the strain paths from points both in annealed conditions and those characterized by an intermediate level of annealing. Nevertheless, when looking at the strain paths along the radial direction, the AH strategy led to a more uniform distribution of strains, since material points at different levels of annealing reached almost the same limit strain (major and minor components). The results from the numerical simulation of the bulge test, combined with those from the plane strain test and tensile tests allowed to cover a wide portion of the forming limit diagram. It must be highlighted that, at this stage, the numerical simulation does not provide direct information about the necking instability and failure behavior due to the absence of a proper modelling of plastic damage. Therefore, the FLD reconstruction here presented should be intended as an investigation about the domain of principal strains that can be achieved by the material points over the whole range of annealing. As a consequence, a qualitative indication of a forming limit diagram could only be drawn.

References

[1] A. Taub, E. De Moor, A. Luo, D.K. Matlock, J.G. Speer, U. Vaidya, Materials for Automotive Lightweighting, Annu. Rev. Mater. Res. 49 (2019) 327–59. https://doi.org/10.1146/annurev-matsci-070218-010134

[2] DIN EN 45545-2. Railway applications - Fire protection on railway vehicles - Part 2: Requirements for fire behaviour of materials and components 2016.

[3] S.S. Hecker, Formability of Aluminum Alloy Sheets, J. Eng. Mater. Technol. 97 (1975) 66-73. https://doi.org/10.1115/1.3443263

[4] G. Palumbo, A. Piccininni, Numerical-experimental investigations on the manufacturing of an aluminium bipolar plate for proton exchange membrane fuel cells by warm hydroforming, Int. J. Adv. Manuf. Technol. 69 (2013) 731–742. https://doi.org/10.1007/s00170-013-5047-1
[5] A. Piccininni, A. Lo Franco, G. Palumbo, Warm Forming Process for an AA5754 Train Window Panel, J. Manuf. Sci. Eng. 144 (2022) 1–12. https://doi.org/10.1115/1.4052583
[6] M. Geiger, M. Merklein, U. Vogt, Aluminum tailored heat treated blanks, Prod. Eng. 3 (2009) 401-410. https://doi.org/10.1007/s11740-009-0179-8
[7] A. Piccininni, G. Palumbo, Design and optimization of the local laser treatment to improve the formability of age hardenable aluminium alloys, Materials 13 (2020). https://doi.org/10.3390/ma13071576
[8] M. Rossi, A. Lattanzi, A. Piccininni, P. Guglielmi, G. Palumbo, Study of Tailor Heat Treated Blanks Using the Fourier-series-based VFM, Procedia Manuf. 47 (2020) 904-909. https://doi.org/10.1016/j.promfg.2020.04.278
[9] M.A. Sutton, J.J. Orteu, H.W. Schreier, Image Correlation for Shape, Motion and Deformation, Springer, 2009.
[10] F. Pierron, M. Grediac, The virtual fields method: Extracting constitutive mechanical parameters from full-field deformation measurements, Springer New York, NY, 2012. https://doi.org/10.1007/978-1-4614-1824-5
[11] S. Avril, M. Bonnet, A.S. Bretelle, M. Grédiac, F. Hild, P. Ienny, F. Latourte, D. Lemosse, S. Pagano, E. Pagnacco, F. Pierron, Overview of identification methods of mechanical parameters based on full-field measurements, Exp. Mech. 48 (2008) 381–402. https://doi.org/10.1007/s11340-008-9148-y
[12] D. Lecompte, S. Cooreman, S. Coppieters, J. Vantomme, H. Sol, D. Debruyne, Parameter identification for anisotropic plasticity model using digital image correlation, Eur. J. Comput. Mech. 18 (2009) 393–418. https://doi.org/10.3166/ejcm.18.393-418
[13] M. Grédiac, F. Pierron, Applying the Virtual Fields Method to the identification of elasto-plastic constitutive parameters, Int. J. Plast. 22 (2006) 602-627. https://doi.org/10.1016/j.ijplas.2005.04.007
[14] M. Rossi, A. Lattanzi, F. Barlat, A general linear method to evaluate the hardening behaviour of metals at large strain with full-field measurements, Strain 54 (2018) 12265. https://doi.org/10.1111/str.12265
[15] M. Rossi, F. Pierron, M. Štamborská, Application of the virtual fields method to large strain anisotropic plasticity, Int. J. Solid. Struct. 97–98 (2016) 322-335. https://doi.org/10.1016/j.ijsolstr.2016.07.015
[16] A. Lattanzi, F. Barlat, F. Pierron, A. Marek, M. Rossi, Inverse identification strategies for the characterization of transformation-based anisotropic plasticity models with the non-linear VFM, Int. J. Mech. Sci. 173 (2020) 105422. https://doi.org/10.1016/j.ijmecsci.2020.105422
[17] J.M.P. Martins, S. Thuillier, A. Andrade-Campos, Calibration of a modified Johnson-Cook model using the Virtual Fields Method and a heterogeneous thermo-mechanical tensile test, Int. J. Mech. Sci. 202–203 (2021) 106511. https://doi.org/10.1016/j.ijmecsci.2021.106511
[18] A. Lattanzi, A. Piccininni, P. Guglielmi, M. Rossi, G. Palumbo, A fast methodology for the accurate characterization and simulation of laser heat treated blanks, Int. J. Mech. Sci. 192 (2021) 106134. https://doi.org/10.1016/j.ijmecsci.2020.106134
[19] A. Piccininni, A. Lattanzi, M. Rossi, Investigation of the plane strain behaviour of a laser-heat treated aluminium alloy Key Engineering Material 926 (2022) 1030-1038. doi:10.4028/p-ic4qyv

[20] A. Piccininni, A. Lattanzi, M. Rossi, G. Palumbo, Investigation of The Anisotropic Behaviour of Laser Heat Treated Aluminium Blanks . Paper presented at ESAFORM 2021. 24th International Conference on Material Forming, Liège, Belgique. (2021). https://doi.org/10.25518/esaform21.4086
[21] F. Grytten, B. Holmedal, O.S. Hopperstad, T. Børvik, Evaluation of identification methods for YLD2004-18p, Int. J. Plast. 24 (2008) 2248-2277. https://doi.org/10.1016/j.ijplas.2007.11.005.
[22] M. Rossi, A. Lattanzi, L. Cortese, D. Amodio, An approximated computational method for fast stress reconstruction in large strain plasticity, Int. J. Numer. Meth. Eng. 121 (2020) 3048-3065. https://doi.org/10.1002/nme.6346
[23] M. Rossi, A. Lattanzi, L. Morichelli, J.M. Martins, S. Thuillier, A. Andrade-Campos, S. Coppieters, Testing methodologies for the calibration of advanced plasticity models for sheet metals: A review, Strain 58 (2022) e12426. https://doi.org/10.1111/str.12426
[24] M. Rossi, A. Lattanzi, F. Barlat, J.H. Kim, Inverse identification of large strain plasticity using the hydraulic bulge-test and full-field measurements, Int. J. Solid. Struct. 242 (2022) 111532. https://doi.org/10.1016/j.ijsolstr.2022.111532
[25] M.G. Oliveira, S. Thuillier, A. Andrade-Campos, Evaluation of heterogeneous mechanical tests for model calibration of sheet metals, J. Strain Anal. Eng. 57 (2021) 208-224. https://doi.org/10.1177/03093247211027061